Advances in Science and Technology Research Journal

Advances in Science and Technology Research Journal, 2025, 19(6), 235–247
https://doi.org/10.12913/22998624/201434
ISSN 2299-8624, License CC-BY 4.0

Received: 2025.02.10
Accepted: 2025.04.15
Published: 2025.05.01

Analysis of the basic aerodynamic characteristics of an unmanned combat aerial vehicle based on a CAD model

Robert Szczepaniak[1*], Zbigniew Czyż[1], Robert Bąbel[1], Amadeusz Mańka[2], Tomasz Zahorski[1], Łukasz Omen[3], Ewelina Kosicka[4], Jonas Matijosius[5], Japhet Noubiap Ngouobe[6]

[1] Polish Air Force University, Faculty of Aviation, Dywizjonu 303 Street No 35, 08-521 Dęblin, Poland
[2] LOT Polish Airlines, Komitetu Obrony Robotników Street No 43, 02-146 Warsaw, Poland
[3] Military University of Technology, Faculty of Mechatronics, Armament and Aerospace Gen. Sylwestra Kaliskiego Street No 2, 00-908 Warsaw, Poland
[4] Lublin University of Technology, Faculty of Mechanical Engineering, Nadbystrzycka Street No 36, 20-618 Lublin, Poland
[5] Vilinius TECH, Laboratory of Experimental Mechanics, Sauletekio al. 11, Vilnius, 10223, Lithuania
[6] Laboratory of Energy, Water, and Environment, National Advanced School of Engineering of Yaoundé, P.O. Box 8390, Yaounde, Cameroon
* Corresponding author's e-mail: r.szczepaniak@law.mil.pl

ABSTRACT

This paper presents an overview of selected unmanned aerial vehicle (UAV) designs to show the development of unmanned aircraft. In this context, the paper describes the application of CAD design in creating a 3D model in order to perform basic aerodynamic CFD simulations. The IAI Heron was selected for geometry modelling. Based on digital analyses of publicly available design materials and photographs, simplified models of the selected structure were created using the SolidWorks software. Basic aerodynamic characteristics of the developed geometric model of the AIA Heron were obtained by calculations made with ANSYS Fluent. The paper analyses the results obtained and compares them to data in the literature for a similar class of UAV. The prepared model will serve as a basis for future 3D prints. The developed CFD numerical model will be used for further comparative analysis and validation in wind tunnel tests.

Keywords: combat drone, IAI Heron, CFD, CAD, aerodynamic characteristics.

INTRODUCTION

Unmanned aerial vehicles are becoming popular and are being used for various applications at an accelerating rate [1, 2]. UAVs are also deployed in various military applications such as surveillance, target tracking, air-to-ground combat, and many others. According to [3], US military spending on UAVs between 2017 and 2021 was estimated at about $17 billion. This paper presents a comprehensive overview of the development of unmanned aerial vehicles (UAVs), with the main focus on the IAI Heron due to its wide application in various civil and military operations. Attention is given to its advanced technological capabilities, which make it an ideal subject for analysis. The method presented and the results obtained provide the basis for developing proprietary know-how and the advancement of research facilities that can be used in the future to design unmanned aircraft. Considering the limited access to detailed design documentation for such aircraft, this approach demonstrates a simplified method for creating a geometrical model. The key contribution lies in assessing its applicability. By analyzing the aerodynamics of the developed aircraft model within the presented scope, this study evaluates whether it is possible

to achieve an object with aerodynamic properties comparable to this class of UAVs.

The first use of unmanned aircraft was observed in 1849 in besieged Venice [4]. The advent of new technologies and propulsion systems along with research into aerodynamics led to the development of many unmanned aircraft at the beginning of the twentieth century. The problem of radio and flight control was solved by two Americans, Peter Cooper and Elmer Sperry, who created the first automatic gyroscopic stabilizer. The stabilizer was used to develop the Navy aircraft N-9 Flying Bomb. This radio-controlled aircraft had an operational range of 80 km and a payload capacity of 135 kg, which makes it a forerunner of today's combat drones. The American company Delco (later part of General Motors Corporation) developed an unmanned aircraft with a wooden fuselage called the Ketterring Bug, which was intended for ground troops [5] (Fig. 1a). Advances in radio control made it possible to operate UAVs in real time. The Curtiss F-5L was the first real-time radio-controlled aircraft [6] to have performed a successful take-off, manoeuvre and landing in September 1924.

Unmanned aircraft were also designed and developed in Great Britain. They were however developed as aerial targets for training, rather than as anti-aircraft defence planes. Examples of aircraft built at that time included: The Aerial Target (an unmanned powered monoplane developed in 1916), the Larynx (it had manned aircraft dimensions and was powered by a Rolls-Royce Lynx engine), and the Fairey Queen (with its design based on the Fairey IIIF). The latter was used in anti-aircraft gunnery training and was a very successful design. The Tiger Moth design was used to devise the second version of the 82B Queen Bee, which was first flown in 1935. The aircraft could operate from runways or ships but landed on water [5]. Launched in 1936, the Dog project involved converting the manned Curtiss aircraft into a radio-controlled unmanned vehicle. The project resulted in the development of a radio-controlled dive bomber in 1938, the Curtiss N2C-2 (Fig. 1b). As part of the test, this aircraft had to torpedo a manoeuvring destroyer using a dummy torpedo. Fleets of aerial targets were also developed, which led to the creation of aircraft such as the Ryan Q-2 Firebee. It was used in ground-to-air and air-to-air gunnery training, as well as for reconnaissance tasks and carrying nuclear warheads [1]. This aerial target played a vital role during the Vietnam War [5] (Fig. 1c). The Q-2 Firebee is the basic type of aerial targets, and its variants include the BGM-34A, BGM-34B, and BQM-34. These models can be considered to be the first unmanned combat aircraft, as they were first used to destroy a ground target using the Maverick missile in December 1971. The Q-2 Firebee is the basic type of aerial targets, and its variants include the BGM-34A, BGM-34B, and BQM-34. These models can be considered to be the first unmanned combat aircraft, as they were first used to destroy a ground target using the Maverick missile in December 1971. It was also observed that due to the lack of a human on board, whose resistance to overloads is low, the aircraft could be used for more violent manoeuvres that were limited only by the strength of the structure (the aircraft could withstand overloads of up to 15G).

Israel is another country with vast experience in the manufacture of UAVs, with the first Israeli-designed UAV being the Mastiff built in 1978 (Fig. 2a.). The aircraft could be used for reconnaissance purposes (this variant was equipped with infrared cameras allowing for near real-time video streaming) or for electronic warfare (its equipment included a radio wave locator and dipole launcher) [5]. Another most notable Israeli-manufactured UAV was the Scout (Fig. 2b).

a) b) c)

Figure 1. a) Kettering Bug [7]; b) Curtiss N2C-2 [8]; c) Two Ryan Q-2 Firebee drones carried under the wing of the C130 Hercules [9]

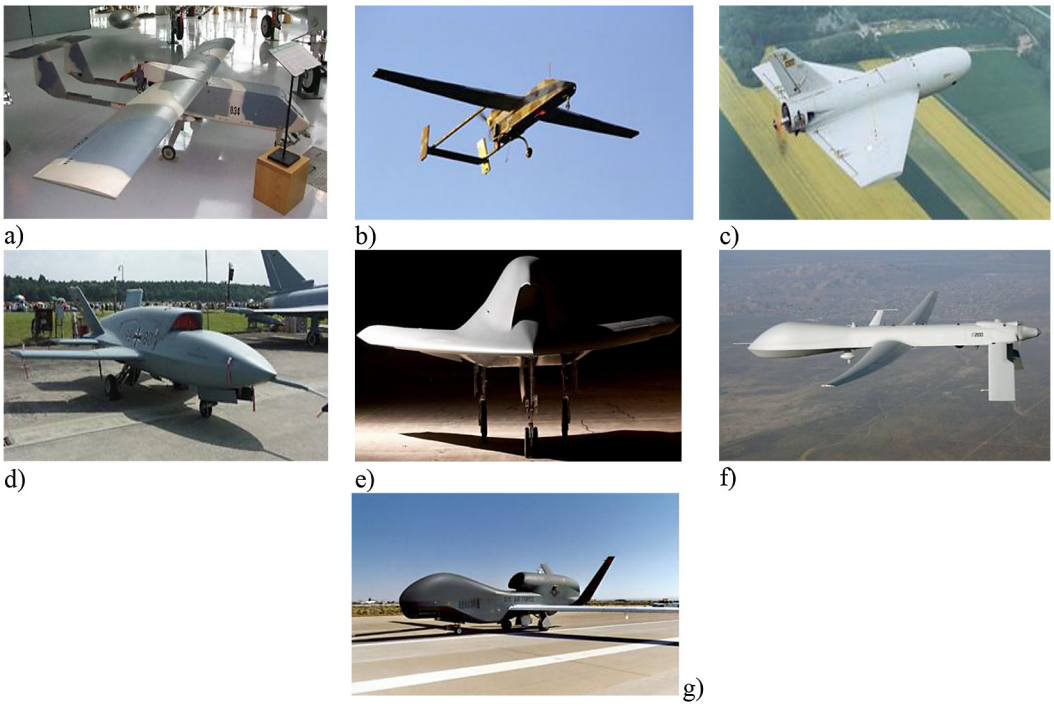

Figure 2. a) Mastiff [11]; b) Scout manufactured by Israel Aerospace Industries [12]; c) Sagem Crecerelle in flight [13]; d) EADS Barracuda [14]; e) NEURON [15]; f) MQ-1 Predator in flight [16]; g) RQ-4 Global Hawk [17]

It was larger than the Mastiff and had enhanced equipment, i.e. flight path and mission data were programmed prior to take-off and could be modified during the flight by the operator. The reconnaissance equipment also included a laser designator for target marking.

France has long been the leading European manufacturer and designer of unmanned aircraft. Various types of UAVs were manufactured in this country. One of these was the Altec MART I, which entered service in 1990 and was used for target location. Another outstanding French-designed UAV was the CAC Fox AT1. This small aircraft system was used in 1993 in Bosnia for 45-minute reconnaissance flights. Based on the experience gained from AT1 operation, the AT2 variant for TX electronic warfare was developed. One of the French UAV manufacturers is the internationally renowned electronics company Sagem. Its best-known UAV, the Crecerelle, is shown in Fig. 2c). Germany is another European country where unmanned aerial vehicles are manufactured. Dornier GmbH developed a vertical take-off sea reconnaissance drone called the Seamos, intended for new-generation frigates. The Seamos drone was used in over-the-horizon surveillance and target location for long-range missiles. Another leading German UAV manufacturer is the Bavarian company ETM which has developed an unmanned aircraft called Luna. A very interesting design developed by German engineers is the EADS Barracuda (Fig. 2d), a jet powered unmanned aerial vehicle. This UAV was first flown in April 2006. The aircraft was constructed predominantly from carbon fibre-reinforced composite material. The only metal component was the wing spar running through the middle and reinforcing the wings. The wing spar allowed for easy removal of the wings for transportation. Also, the specially shaped fuselage made it possible to scatter radar waves, thus making the Barracuda drone difficult to detect on foreign radars.

This project continues to be developed, with its main competitor being a project called *NEURON* that was launched by the French Dassault Aviation company (Fig. 2e). In the US, General Atomics have built several state-of-the-art unmanned aerial vehicles, including the Gnat 750, RQ-1 Predator, Dark Star, and Global Hawk. The Gnat is used for training purposes. The RQ-1 Predator (Fig. 2f), on the other hand, is an excellent aerial reconnaissance platform. It is equipped with an imaging system for real-time observation of the target. The RQ-1 is also provided with optoelectronic devices such as two TV cameras, an infrared system and laser designator, which makes reconnaissance possible in poor weather conditions. The RQ-1 is an excellent example of a tactical-level UAV. Over time, however, a need emerged for high-altitude,

long-endurance unmanned aircraft that would be equipped with even more precise electronic devices (for both mapping as well as sending and processing of data). This led to the development of the RQ-4 Global Hawk (Fig. 2g), which made its first flight in January 1998 and was delivered to the US Army the following year [10].

Unmanned aerial vehicles (UAV) have been used primarily in the military for reconnaissance and targeting, but in recent years they have been used extensively in agriculture, fishing, weather observation, communication, and entertainment. In this section, we will discuss the most promising emerging applications of UAV according to their potential market value (Fig. 3 and 4). Unmanned aerial vehicles (UAV) have been used primarily in the military for reconnaissance and targeting, but in recent years they have been used extensively in agriculture, fishing, weather observation, communication, and entertainment. In this section, we will discuss the most promising emerging applications of UAV (Fig. 3) according to their potential market value.

The increasing utility of drones leads to a proportional rise in their financial impact. Pricewaterhouse Coopers [18] predicts that the potential market value of business services that can benefit from drone technology will reach several billion dollars across various industries (Fig. 4). The most promising applications of drones and their market potential have been discussed in detail in the publication.

THE IAI HERON MODEL AND METHOD

The paper discusses the use of CAD design in creating a 3D model to perform basic aerodynamic CFD simulations. For this purpose, ANSYS Fluent – one of the most widely used tools for simulating airflows and analyzing the aerodynamic characteristics of aircraft – was utilized. Fluent provides a wide range of models for turbulence, multiphase flow, and chemical reactions, enabling engineers to accurately simulate complex flow conditions around the aircraft. This allows for precise prediction of aerodynamic characteristics, such as lift and drag forces, across a wide range of speeds, angles of attack, and other parameters relevant to aircraft performance.

Nevertheless, researchers are seeking alternatives that are either less costly or faster. In [19],

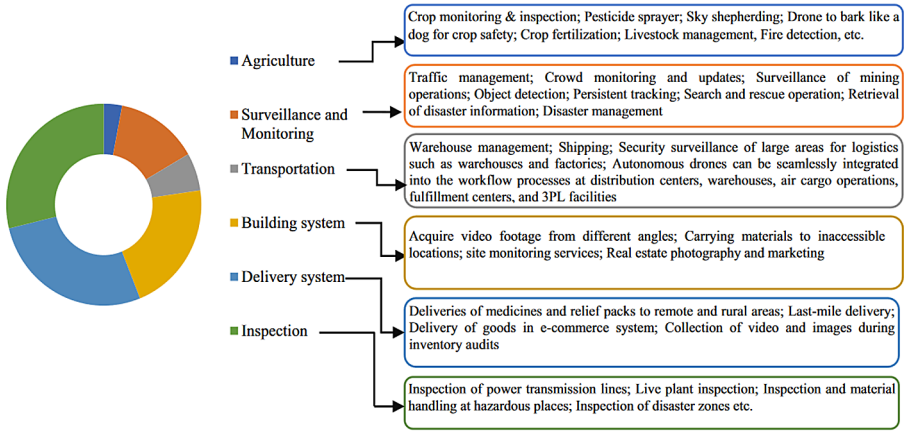

Figure 3. Applications of UAV

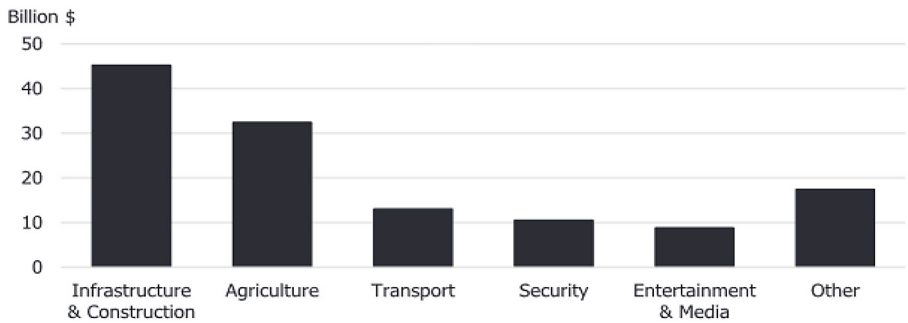

Figure 4. Potential market value of commercial drone applications [18]

a method is presented that enables the estimation of aerodynamic forces and moments acting on irregularly shaped projectile fragments during their flight through the atmosphere. The main objective of their study was to develop a mathematical model that could replace time-consuming CFD simulations (such as those conducted with ANSYS Fluent) while maintaining high accuracy. The authors performed CFD simulations in Fluent to obtain aerodynamic data for projectiles, which were then used to validate the results of the proposed mathematical model. In [20], the authors attempted to model submarine drag using FS in the ABAQUS environment and the results were compared to values carried out on the ship. Other ways of determining lift and drag forces can be in-house computational methods such as in the work [21]. In contrast, ANSYS Fluent plays a key role in the numerical simulations in [22], which focus on flow analysis around projectiles and the study of supercavitation phenomena, crucial for reducing drag in water. Research on the aerodynamic characteristics of corrugated airfoil surfaces demonstrates that such a surface increases drag but delays flow separation at low Reynolds numbers, as shown in [23] using ANSYS Fluent. In this study, the aerodynamic characteristics of an airfoil with angled baffles were verified, and the flow field at various angles of attack was solved using CFD based on the Reynolds-averaged Navier-Stokes (RANS) equations.

The IAI Heron (Machatz-1)

The potential of using CAD software for UAV geometry reconstruction is illustrated through an example of the IAI Heron. This unmanned aerial vehicle (Fig. 5a) was developed by the Malat division of Israel Aerospace Industries. The UAV is capable of medium altitude long endurance (MALE) operations and has demonstrated 52 hours of continuous flight at up to 13 000 m. The F-Heron TP version was purchased by the French Air Force, and under technology transfer is now produced by the French group Dassault. The aircraft was supposed to fill the gap between previously unmanned aerial vehicles and new-generation manned aircraft that were developed as part of the agreement between Dassault and British Aerospace under the Telemos programme [10]. The general characteristics for the IAI Heron are summarized in Table 1.

The Heron can carry a variety of payloads, including electro-optical/infrared (EO/IR) cameras,

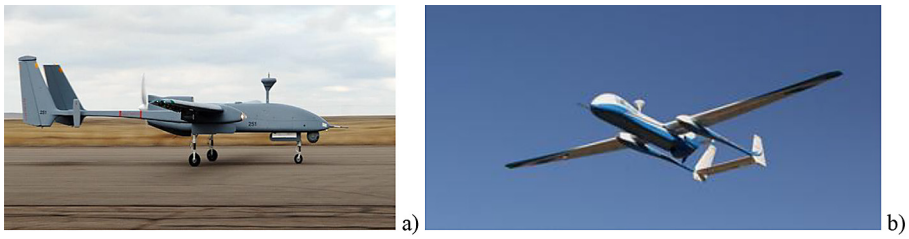

a) b)

Figure 5. IAI Super Heron: a) basic version [25]; b) the latest version of the Israeli-manufactured Heron UAV [26]

Table 1. The general characteristics for the IAI Heron [24]

Technical parameter	Value
Nominal take off weight	1100 kg
Max. useful load (fuel and payload)	500 kg
Max fuel weight	400 kg
Max. payload weight	250 kg
Basic empty weight	600 kg
Length	8.58 m
Wing span	16.6 m
Engine	Rotax 914 four-cylinder engine
Cruise speed	130–150 km/h
Maximum speed	207 km/h
Endurance	Up to 52 hours (depending on mission profile and payload)
Range	350 km with line-of-sight communication, and up to 1000 km with satellite communication

synthetic aperture radar (SAR), communication intelligence (COMINT), and electronic intelligence (ELINT) systems. It is primarily used for intelligence, surveillance, and reconnaissance (ISR) missions. It can be equipped for target acquisition, maritime patrol, and even tactical communication relay. The Heron has been widely adopted by several countries due to its versatility and advanced capabilities in various military and civilian operations.

This aircraft has a distinctive design with a double tail boom. Between the booms is the fuselage, and in the rear fuselage is mounted a pusher propeller driven by a 115 hp piston engine, and in its advance version, the Heron TP (also known as the IAI Eitan), which is much bigger than the regular Heron – by a 1200 hp turbine engine. The aircraft is also equipped with a de-icing system. The aircraft has a tricycle undercarriage, with a retractable nosewheel. The Heron can operate in any weather conditions. This aircraft uses a multi-sensor reconnaissance suite, including SIGINT, COMINT, ELINT, and other radar systems. The aircraft is capable of autonomous flight, take-off and landing; however, it can also be manually controlled from a ground control station. Thanks to the triple-redundant avionics, the UAV is reliable enough to fly over urban areas without any problems. An integral GPS receiver is used for navigation, which allows the flight to be performed in compliance with the pre-programmed flight profile [10].

The latest version of this UAV is the IAI Super Heron (Fig. 5b) powered by a 200 hp diesel engine. Compared to the original Heron version, it has a 5% reduced aerodynamic drag and improved performance (maximum speed and climb rate).

Classifying drones is a challenging task, as the criteria vary between countries. Unmanned aerial vehicles (UAV) can be categorized based on three criteria: cruising altitude, endurance in terms of flight time, main drone dimensions [27]. These classifications typically include tactical drones, medium-altitude long-endurance UAVs (MALE), and high-altitude long-endurance UAVs (HALE). According to this classifacation, the IAI Heron (Machatz-1) is capable of medium altitude long endurance (MALE).

Design of the IAI Hron

The CAD design process involves creating 2D or 3D objects in computer environment that reflect actual structures [28]. As a result, it is possible to generate a 3D visualisation of a given structure before it is even created. In addition to that, the CAD software makes it possible to define materials used to create the object for strength analysis [29, 30], optimising or simulating flow around the model [31–34], which significantly reduces the costs associated with creating a real model and conducting experiments. Once a CAD design of the aircraft has been made, it is possible to create the model by 3D printing for further tunnel (aerodynamic, hydrodynamic) tests [35–37], as well as for load tests [38, 39] and even thermal tests [40], in order to optimise the design.

In this study, the UAV model was designed using SolidWorks. Parts were mainly created by converting a 2D sketch or several 2D sketches so as to obtain the desired 3D shape (Fig. 6a). Thanks to this software, it was possible to create multi-object models by means of assemblies (Fig. 6b) and the conversion of the finished design to an engineering drawing, where each part of the assembly can be visualized as projections and sections, as well as can be dimensioned. For the purpose of this study, high-quality photographic images of a combat drone were rendered using PhotoView360 tools (Fig. 6c, 6f). Figure 6a shows the basic orthographic projections used to create the 3D model, which were developed on the basis of [24].

The sketch picture option in SolidWorks was used for model design. First, a fuselage model was created, starting with the nose. It was created using the extrude command. To create the desired nose shape, the part was divided into three segments – the top, bottom and central ones. Sketches of each segment were made, and then a point was sketched on the added plane. On the right-hand plane, the upper and lower guide paths were created. Using the 3D sketches, lateral guide paths were created. The first step was to extrude the upper segment of the nose. After that, the bottom segment was extruded. The final step was to extrude the surface between the walls that were formed as a result of the above operations (Fig. 6a). The Heron wing is based on an advanced aerodynamic slotted airfoil (SA-21) developed by IAI. The wings of the object under study were drawn based on simplified sketches in the paper [24].

CFD calculations

The created model was used to perform a numerical aerodynamic analysis with minor

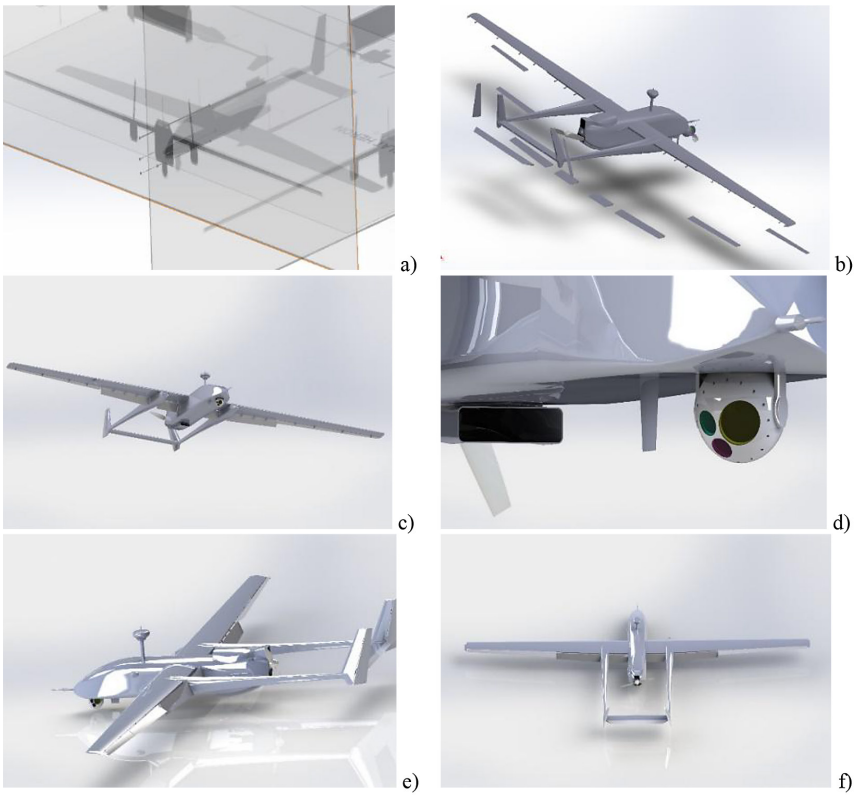

Figure 6. IAI Heron- a) sketch picture, b) exploded view, c) with flap displacement – bottom view, d) fuselage bottom part with visible moveable optoelectronic head and air inlet, e) with flap displacement – left-hand side view, f) rear view

simplifications in order to correctly generate computational meshes for numerical calculations (Fig. 7). The meshes were generated in the Ansys Meshing module by selecting the appropriate element sizes according to the characteristic dimensions of the calculational domain. The meshes were generated by the tetrahedrons meshing method with the patch conforming algorithm. A boundary layer consisting

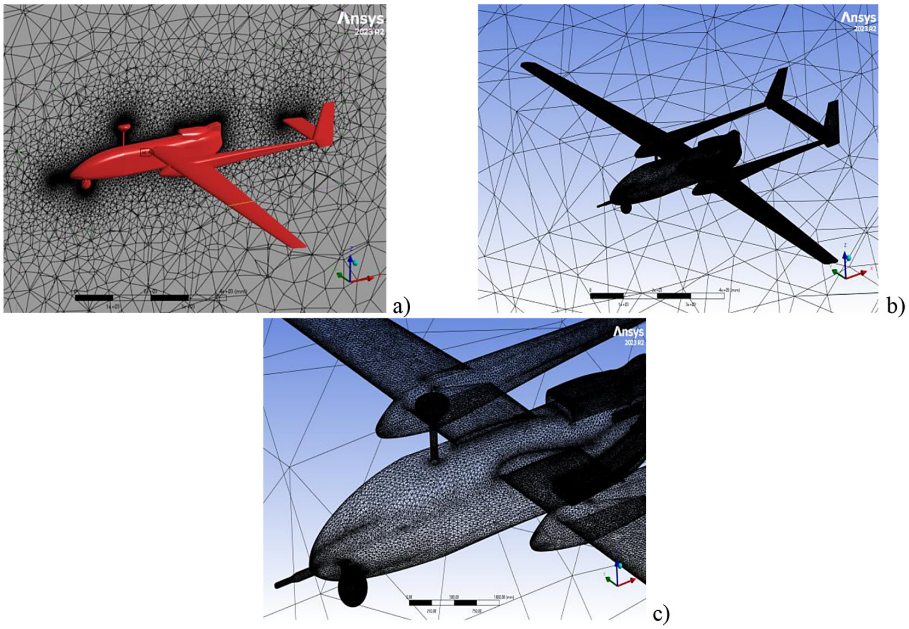

Figure 7. a) View of the mesh on the symmetry plane for the applied computational domain b) General view of the mesh on the surface of the entire test object; c) Mesh on the surface of the test object – view of the fuselage front part

of 5 layers was defined on the wall surface using the smooth transition option. The maximum skewness coefficient of the generated meshes did not exceed 0.96. The thickness of the boundary layer was determined based on the flow type measured by the Reynolds number. The generated mesh consisted of 5,004.438 elements with 1,304.331 nodes. Meshing plays a very important role in CFD simulations because the accuracy of results depends on the mesh type and quality. Examples of the generated meshes are shown in Figures 7a–7c.

Calculations were made for a 3D turbulent steady flow using the finite volume method-based Ansys Fluent software. Pressure and velocity equations were solved by the coupled method. Second order upwind differential equations were used for the spatial discretization of turbulent kinetic energy, turbulent dissipation rate, energy and pressure equations.

For the numerical analysis, a k-ω SST (shear stress transport) turbulence model was selected. The model introduces two additional transport equations into the system of averaged Navier-Stokes equations: one for turbulent kinetic energy and the other for specific dissipation rate. The k-ω SST turbulence model was chosen because of its relatively accurate representation of turbulence in the boundary layer, as well as due to its low sensitivity to the boundary conditions of turbulence at the inlet. The next step involved assigning boundary conditions. The CFD geometric model had one inlet and one outlet. The air inlet to the computational domain was set as a velocity-inlet of 57.5 m/s. The domain outlet was set as a pressure-outlet, and the outlet pressure was the standard atmospheric pressure. Physical parameters such as air density and viscosity were set for a temperature of 288 K and made equal to 1.2257 kg/m^3 and 1.7894 × 10^{-5} kg/(m·s), respectively.

RESULTS AND DISCUSSION

Results

The numerical results were used to prepare aerodynamic characteristics of the analysed model. The origin of the coordinate system for determining the moments was defined at the quarter-chord point (25% of the length) of the mean aerodynamic chord (MAC). Figurte 8a shows the aerodynamic forces acting on the tested object as a function of the angle of attack for a sideslip angle β of 0°. Figure 8b shows the results of aerodynamic

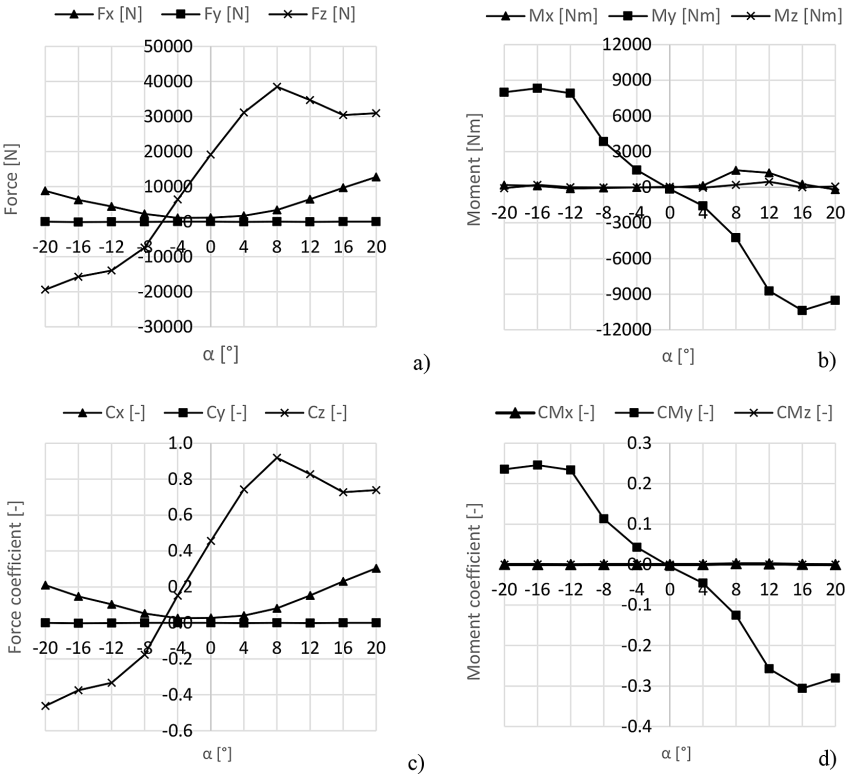

Figure 8. a) Force as a function of the angle of attack α; b) Moment as a function of the angle of attack α; c) Force coefficient as a function of the angle of attack α; d) Moment coefficient as a function of the angle of attack α

moments acting on the tested object. The results show that the drag force first decreases from α = -20° to α = -4°, reaching its minimum value at α = -4°, and then increases from α = -4° to α = 20°. This trend suggests that the aircraft experiences a reduced drag with decreasing the angle of attack from α = -20° to α = -4°, after which the drag increases as the angle of attack is increased from α = -4° to α = 20°. The side force (Fy) remains minimal over the entire range of the angle of attack, ranging from -111.52 N to 7.64 N. The changes are small and oscillate around zero, which suggests that the angle of attack has a minimal impact on the side force at a sideslip angle β equal to 0°. The lift force (Fz) shows a clear increasing trend, from negative values at negative angles of attack to positive values at positive angles. The lift increases with the angle of attack, reaching the maximum value around α = 8°, and afterwards it gently decreases but still remains high.

The rolling moment (Mx) shows non-zero values as a function of the angle of attack despite a symmetrical flow. It changes sign several times, which suggests the occurrence of complex aerodynamic interactions as a function of the angle of attack. Nevertheless, the value of this moment is low relative to the principal pitching moment My. A similar situation can be observed for the Mz moment. The pitching moment My shows a decreasing trend in a range from α=-16° to α=+16°, which indicates that the test object-maintained stability at these angles of attack. Figures 8c and 8d show the coefficients of force and moment, respectively. The coefficients were calculated for a wing span of 16.66 m, mean aerodynamic chord of 0.81 m and gross area of 20.67 m^2.

Figure 9 shows two characteristics. The first is the lift-drag ratio as a function of the angle of attack α and the second is the polar curve of the IAI Heron aircraft model. Their analysis shows that the maximum value of Cz/Cx is 18.36 and occurs at an angle of attack of 4°. This is the point at which the aircraft achieves the highest aerodynamic efficiency, i.e. the greatest distance per unit of drag. It can be concluded that the aircraft has good aerodynamics in the angle range from 0° to 8°. Above this value, the drag increases too fast relative to the lifting force.

Figure 10 shows the pressure contours on the surface of the test object and the velocity contours around the test object on the symmetry plane, respectively. The images are shown for selected extreme angles of attack, i.e. α=-20°, α=0° and α=20°. The pressure distribution and airflow around the aircraft strongly depend on the angle of attack (α). At negative angles of attack, the pressure on the upper surface of the wing is higher than at a zero angle of attack because the airflow is directed more downwards, which leads to reduced flow velocity and increased pressure. On the lower surface of the wing, the pressure is lower than at a zero angle of attack because the airflow flows around the wing at a greater angle, which leads to increased flow velocity and reduced pressure. At negative angles of attack, the airflow around the wings is less effective. At high negative angles of attack, flow separation may occur, leading to increased drag and reduced absolute lift. The airflow around the fuselage and stabilisers is more turbulent. Disturbed flow can occur on the tail plane, which affects the stability and controllability of the aircraft. This is indicated by the range below α =-16° where the moment coefficient derivative dCMy due to α shows positive values, which results in lack of stability for these large negative angles. It should be noted that this derivative reaches negative values for a relatively large range of angles of attack from α =-16° to α =16°. In this range, it can be considered that the object maintains longitudinal stability.

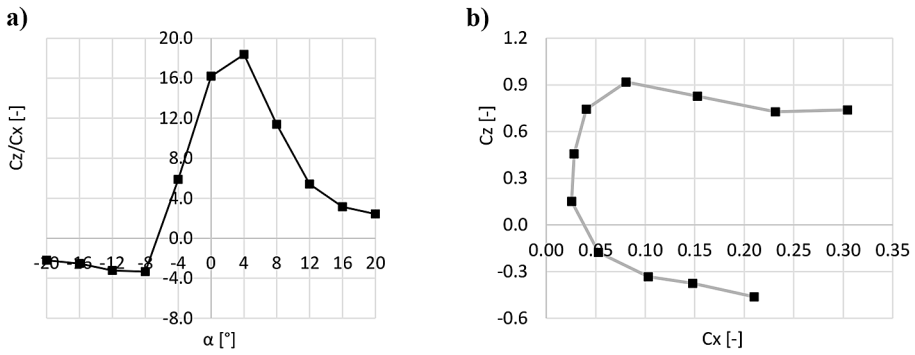

Figure 9. a) Lift-drag ratio as a function of the angle of attack α; b) Drag polar of the IAI Heron aircraft model

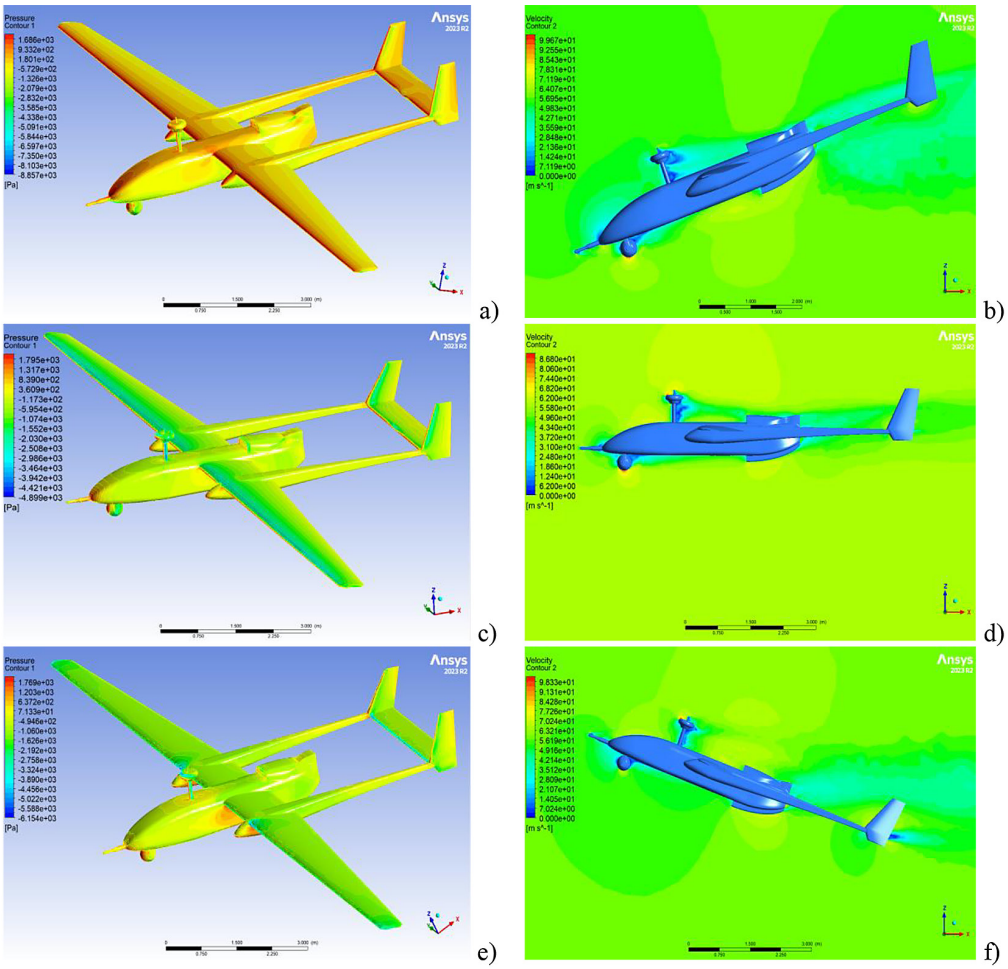

Figure 10. a) Pressure contour on the surface of the test object for α=-20° and β=0°; b) Velocity contour on the symmetry plane of the test object for α=-20° and β=0°; c) Pressure contour on the surface of the test object for α=0° and β=0°; d) Velocity contour on the symmetry plane of the test object for α=0° and β=0°; e) Pressure contour on the surface of the test object for α=20° and β=0°; f) Velocity contour on the symmetry plane of the test object for α=20° and β=0°Discussions

At positive angles of attack the pressure on the upper surface of the wing is lower than at a zero angle of attack because the airflow around the wing is at a higher angle, leading to increased flow velocity and reduced pressure. This results in increased lift. On the lower surface of the wing, the pressure is higher than at a zero angle of attack because the airflow is directed more upwards, leading to reduced flow velocity and increased pressure.

At positive angles of attack, the airflow around the wings is more efficient, which leads to increased lift. However, at very high angles of attack, flow separation occurs from the upper surface of the wing, leading to increased drag and causing stall. The flow around the fuselage and tail planes is more beneficial for generating lift and ensuring flight stability. The lift on the tail plane is higher, which helps to maintain the airplane's stability. In Figure 10f one can notice an aerodynamic trace behind the fuselage which does not disturb the flow around the tail plane as much as it does at high negative angles.

Discussion

According to literature data [41, 42] typical Cz/Cx values for fighter aircraft range from 8 to 12, and for drones of the MALE class, to which IAI Heron may be classified, these values range from 20 to 25. The result obtained from calculations Cz/Cx=18.36 suggests that the aircraft has aerodynamics similar to that class of drones. However, it should be recognised that the difference obtained is not that large. Compared to the Cz/Cx=20 value, this is only about 8% difference. It can be considered that the developed aircraft model has a very good aerodynamic efficiency in

its operational range. However, if we were to justify the difference obtained, it may be primarily due to some differences in design and wing airfoil. As there is no accurate data of the IAI Heron aircraft in the literature, it can also be assumed that the method used represents its performance very well and that in reality the object under test does not reach Cz/Cx values above 20 but much less. This can be illustrated, for example, by the results presented in paper [43] where a similar class of aircraft was studied. It presents Cz/Cx values in the range of angles of attack α from -4° to 8°. The maximum value was reached at around Cz/Cx = 17. This confirms that this type of aircraft does not need to reach values above 20, especially when it comes to military use.

Although studies are being conducted on modifying the existing combat drones [33], it should however be remembered that the developed models are most often simplified due to the secrecy of aircraft documentation, as well as due to the requirements for computational models and 3D prints. Nonetheless, the use of modelling based on sketches and demonstrative photographs, the effect of which is described in this paper, makes it possible to create 3D models for numerical analysis or to produce a real object that is scaled for the needs of particular equipment. Numerical modelling of aircraft requires paying particular attention to the accuracy of reproducing aircraft shape and airflow conditions. More complex models can be time-consuming and expensive to develop and simulate. Therefore, it is important to use the simplest possible methods that will provide a sufficient level of accuracy and ensure agreement of numerical results with reality. The main aspects that had to be considered in this study were model geometry and computational mesh. Although simplified models (e.g. solids of basic shapes) are quick and easy to develop, they may not consider all the key elements affecting airflow. More detailed models (with detailed representation of wings, fuselage, stabilisers) are more difficult to create but provide more accurate results. A less dense mesh is simpler to calculate, but it may result in greater calculation errors. On the other hand, a denser mesh ensures higher accuracy of the results, but its application requires more computational resources. It is therefore vital that individual factors be optimized in this type of studies. Also, simplified conditions may not reflect real aviation situations. More accurate conditions require more data and complex calculations, but they better reflect reality. The findings will be used in future studies aimed at identifying the differences between results obtained from simple and more complex models. This will provide additional insight into the impact of modelling simplifications on the accuracy of obtained results. It is important to find a compromise between the simplicity of the model and the accuracy of the results, and to develop a methodology that allows the most efficient numerical modelling with the required accuracy.

CONCLUSIONS

The results obtained provided a better understanding of the aerodynamics of the aircraft under consideration and can be used to assess its operational capabilities, inspire design improvements, and explore potential technologies. Based on these results, a comparison was made with existing aircraft in terms of performance and aerodynamic characteristics. This paper presents the results of numerical aerodynamic calculations for the model analysed. The results show realistic trends and the analysed object shows stability in the angle of attack range from α=-16° to α=+16°. The obtained value Cz/Cx = 18.36 suggests that the aircraft model has a very good aerodynamic efficiency, close to the MALE class drones, indicating its good performance in the operational range. The difference between the obtained result and the value reported in the literature is small (about 8%), which may be due to design differences such as the airfoil of the wing. However, it is difficult to find the precise reasons due to the lack of data on the IAI Heron in the literature.

The analysis conducted will inspire future designs, and the developed geometry for CFD calculations can also be used to evaluate potential stealth technologies through shape and airflow analysis. It is possible to determine whether the design has been optimized to minimize detectability; however, this is not the focus of this work. The outcome of this work is the creation of a CAD model for numerical calculations, which can later be printed using rapid prototyping technology, e.g., for wind tunnel tests. The model was created based on three basic views (right view, top view, front view) imported into SolidWorks, as well as reference photographs. Due to the lack of access to the actual object and detailed design plans, some of the details are indicative in nature.

This project may undergo further modification and improvement. Future studies will focus on the development of hybrid modelling methods that combine simplicity and accuracy, as well as the validation of numerical results with experimental data. They may include the use of machine learning algorithms to predict aerodynamic behavior based on previous simulations and experiments. The applied theoretical aerodynamic models can also be calibrated using data from wind tunnel tests or flight tests.

Additionally, efforts will be directed toward optimizing numerical algorithms and meshing techniques to achieve higher accuracy with less computational effort. Another key area of focus will be the topological optimization of UAVs based on hybrid composites, with the goal of predicting the percentage of weight reduction in a UAV structure made of bamboo composites using optimization strategies. The ultimate outcome of these studies will be the development of simple yet accurate numerical modelling methods for the rapid and reliable prediction of aerodynamic characteristics and aircraft performance, which is crucial for effective engineering design and analysis.

Acknowledgments

This work was prepared in part during an international scientific internship undertaken by Robert Szczepaniak, Zbigniew Czyż and Tomasz Zahorski from Polish Air Force University (Poland) international scientific internship at the Institute of Mechanical Science of Vilnius Gediminas Technical University. The internship took place from August 16 to September 16, 2024.

REFERENCES

1. Liu Y, Dai H-N, Wang Q, Shukla MK, Imran M. Unmanned aerial vehicle for internet of everything: Opportunities and challenges. Comput Commun 2020;155:66–83. https://doi.org/10.1016/j.comcom.2020.03.017
2. Vashisht S, Jain S, Aujla GA, Mac protocols for unmanned aerial vehicle ecosystems: Review and challenges, Comput Commun. 2020;160:443–463. https://doi.org/10.1016/j.comcom.2020.06.011
3. Drones: Reporting for work, https://www.goldmansachs.co m/insights/technology-driving-innovation/drones/ [accessed 15 May 2021].
4. Chamola V, Kotesh P, Agarwal A, Naren, Gupta N, Guizani M. A comprehensive review of unmanned aerial vehicle attacks and neutralization techniques, Ad Hoc Netw. 2021;111:102324. https://doi.org/10.1016/j.adhoc.2020.102324
5. Karpowicz J, Kozłowski K. Unmanned Aerial Vehicles and Miniature Flying Devices. Possibilities and Scope of Use in Military Operations, Warsaw: National Defense University; 2003 [in Polish].
6. Keane J, Carr S, A brief history of early unmanned aircraft, Johns Hopkins Apl Technical Digest. 2013; 32: 558–571.
7. Kettering Bug w National Museum of the United States Air Force, http://i208.photobucket.com/albums/bb284/armyjunk1/Wright-Patterson%20AF%20Museum/Early%20Years/0151.jpg (accessed 15 November 2016).
8. USN version of Fledgling as trainer. http://aerofiles.com/_curtx.html [accessed 12 April 2024).
9. https://upload.wikimedia.org/wikipedia/commons/thumb/8/88/DC-130_mounted_Firebees_DN-SC-85-06043.jpg/220px-DC-130_mounted_Firebees_DN-SC-85-06043.jpg [accessed 15 April 2024].
10. Adamski M., Rajchel J. Unmanned Aerial Vehicles, Part I. Characteristics and Use, Dęblin: Air Force Academy; 2013 [in Polish].
11. Mastiff, http://www.wiichat.com/attachments/usmc-mastiff-iii-uav-jpg.4627.jpg?/ [accessed 15 May 2024].
12. http://www.iai.co.il/2013/36755-43199-en/MediaRoom.aspx [accessed 15 May 2024].
13. http://www.safran-electronics-defense.com/sites/sagem/files/styles/landscape_medium/public/thumbnails/image/1996_1er_vol_du_drone_crecerelle.jpg?itok=M3y8laqv [accessed 15 May 2024].
14. https://upload.wikimedia.org/wikipedia/commons/thumb/a/a4/Barracuda_av_dr.jpg/1280px-Barracuda_av_dr.jpg [accessed 15 May 2024].
15. https://www.dassault-aviation.com/en/defense/neuron/ [accessed 15 May 2024].
16. http://www.uasvision.com/wp-content/uploads/2013/05/predator.jpg [accessed 16 May 2016].
17. http://www.northropgrumman.com/Photos/pgL_GH-10020_021.jpg [accessed 15 May 2024].
18. Mazur M., McMillan J., Wisniewski A. Clarity from above. PwC global report on the commercial applications of drone technology, Tech. report, PricewaterhouseCoopers, 2016.
19. Kljuno E., Catovic A. A generalized model for estimation of aerodynamic forces and moments for irregularly shaped bodies, Def Technol 2019: 15(3): 369–389, https://doi.org/10.1016/j.dt.2018.09.006
20. Kiciński R, Jurczak J. Submarine Resistance Force Characteristics Determination after Modification of Depth Rudder System. Adv. Sci. Technol. Res. J. 2021; 15(1): 1–9, https://doi.

org/10.12913/22998624/125186.

21. Grządziela A. P., Kraskowski M., Król P., Szturomski B. J., Kiciński R. Experimental Validation of an FEM Model Based on Lifting Theory Applied to Propeller Design Software. Polish Maritime Research, https://doi.org/10.2478/pomr-2024-0022
22. Huang X. Cheng C, Zhang X, Machine learning and numerical investigation on drag reduction of underwater serial multi-projectiles, Def Technol 2022; 18(2): 229–237, https://doi.org/10.1016/j.dt.2020.12.002
23. Ma N, Liu L, Meng F, Meng J. Structural design and modal behaviors analysis of a new swept baffled inflatable wing, Def Technol 2023;24:382–398, https://doi.org/10.1016/j.dt.2023.02.004
24. Ernst J., Tsach S., Penn D. Evolution of the heron UAV family. American Institute of Aeronautics and Astronautics, Inc., Virginia, 2005.
25. http://www.avionslegendaires.net/wp-content/uploads/images/avion_militaire/Gheron-index.jpg [accessed 21 May 2024].
26. http://cdn.i24news.tv/upload/image/_Super%20Heron.jpg [accessed 21 May 2024].
27. Arjomandi M. Aeronautical engineering classification of unmanned aerial vehicles. 2016. https://web.archive.org/web/20121021021237/http://personal.mecheng.adelaide.edu.au/maziar.arjomandi/aeronautical%20engineering%20projects/2006/group9.pdf [accesed in 08.02.2025].
28. Domino J, Czyż Z, Bąbel R. Aerodynamic Load Measurements on the Example of Diamond DA42 Model Aircraft. IEEE 10th International Workshop on Metrology for AeroSpace, 2023; 704–708, https://doi.org/10.1109/MetroAeroSpace57412.2023.10189976
29. Milewski S., Szturomski B., Kicinski R. Strength Analysis of the Marine Weapon's Construction. NASE MORE. 2021; 68(3): 167–174. https://doi.org/10.17818/NM/2021/3.4
30. Kicinski R. Szturomski B., Marchel L. A more reasonable model for submarines rescues seat strength analysis. Ocean Engineering. 237. https://doi.org/10.1016/j.oceaneng.2021.109580
31. Stryczniewicz K, Stryczniewicz K, Szczepaniak R. Modelling hydrodynamic characteristics of the underwater glider based on Computational Fluid Dynamics, 2019 IOP Conf Ser: Mater Sci Eng. 2019; 710: 012012. https://doi.org/10.1088/1757-899X/710/1/012012
32. Szczepaniak R, Bąbel R, Grzywacz A, Stryczniewicz W, Kowaleczko G. The effect of using the kline-fogleman modification upon the coefficient characterics of aerodynamic forces in the airfoil. J Kones 2018; 25(2): 349–355. https://doi.org/10.5604/01.3001.0012.2854
33. Zahorski T, Konopka B, Stryczniewicz W, Bąbel R, Szczepaniak R. CFD Analysis of the Influence of Flaps Extension on Aerodynamic Characeristics of M-28 Bryza Aircraft. J Kones 2016; 23(1): 353–360.
34. Ganesan T, Jayarajan N. Aerodynamic Analysis of Mathematically Modelled Propeller for Small UAV Using CFD in Different Temperature Conditions. Stroj vestnik-J Mech E, 2023; 69(11–12): 444–454. http://dx.doi.org/10.5545/sv-jme.2023.601
35. Stryczniewicz W, Placek R, Szczepaniak R. Piv Measurements of Flow Separation Over Lamiar Airfoil at Transonic Speeds. J Kones 2016; 23(1): 329–336.
36. Czyż Z, Jakubczak P, Podolak P, Skiba K, Karpiński P, Droździel-Jurkiewicz M, Wendeker M, Deformation measurement system for UAV components to improve their safe operation, Eksploat Niezawod-Maintenance and Reliability 2023: 25(4). http://doi.org/10.17531/ein/172358
37. Filipiak D, Szczepaniak R, Zahorski T, Bąbel R, Stabryn S, Stryczniewicz W. Flow visualization over an airfoil with flight control surfaces in a water tunnel. Transactions on Aerospace Research 2017; 246(1): 63–78.
38. Czyż Z, Podolak P, Skiba K, Jakubczak P, Karpiński P, Różyło P, Droździel-Jurkiewicz M. Autogyro Main Rotor Blade Strength Tests. IEEE 10th International Workshop on Metrology for AeroSpace 2023; 199–204. https://doi.org/10.1109/MetroAeroSpace57412.2023.10190031
39. Brazhenko V, Qiu Y, Cai J, Wang D. Thermal Evaluation of Multilayer Wall with a Hat-Stringer in Aircraft Design. Stroj vestnik-J Mech E, 2022; 68(10): 635–641. http://dx.doi.org/10.5545/sv-jme.2022.222
40. Bagul P, Rana ZA, Jenkins KW, Konozsy L, Computational engineering analysis of external geometrical modifications on MQ-1 unmanned combat aerial vehicle. Chinese J Aeronaut 2020; 33(4): 1154–1165 https://doi.org/10.1016/j.cja.2019.12.027
41. Raymer D. P. Aircraft Design: A Conceptual Approach. American Institute of Aeronautics and Aerodynamics - Education Series, 5th Edition, 2012.
42. Anderson J., Bowden M. Introduction to Flight ISE - 9th Edition. McGraw-Hill Education, 2021.
43. Haoqin S., Xiaoxiang B., Jianhua L., Kai L., Mengxi C., Jing S. Calculation and Analysis on Stealth and Aerodynamics Characteristics of a Medium Altitude Long Endurance UAV. Procedia Engineering2015; 99, 111–115.